J Mater Sci (2018) 53:2604–2617

Computation

Molecular dynamics-based multiscale damage initiation model for CNT/epoxy nanopolymers

Nithya Subramanian[1,*], Bonsung Koo[1], Ashwin Rai[1], and Aditi Chattopadhyay[2]

[1] Arizona State University, 551 E. Tyler Mall, Tempe, AZ 85287, USA
[2] Mechanical and Aerospace Engineering, Arizona State University, 551 E. Tyler Mall, Tempe, AZ 85287, USA

Received: 1 June 2017
Accepted: 19 October 2017
Published online: 26 October 2017

ABSTRACT

A methodology that accurately simulates the brittle behavior of epoxy polymers initiating at the molecular level due to bond elongation and subsequent bond dissociation is presented in this paper. The system investigated in this study comprises a combination of crystalline carbon nanotubes (CNTs) dispersed in epoxy polymer molecules. Molecular dynamics (MD) simulations are performed with an appropriate bond order-based force field to capture deformation-induced bond dissociation between atoms within the simulation volume. During deformation, the thermal vibration of molecules causes the elongated bonds to re-equilibrate; thus, the effect of mechanical deformation on bond elongation and scission cannot be captured effectively. This issue is overcome by deforming the simulation volume at zero temperature—a technique adopted from the concept of quasi-continuum and demonstrated successfully in the authors' previous work. Results showed that a combination of MD deformation tests with ultra-high strain rates at near-zero temperatures provides a computationally efficient alternative for the study of bond dissociation phenomenon in amorphous epoxy polymer. In this paper, the ultra-high strain rate deformation approach is extended to the CNT-epoxy system at various CNT weight fractions and the corresponding bond disassociation energy extracted from the simulation volume is used as input to a low-fidelity continuum damage mechanics (CDM) model to demonstrate the bridging of length scales and to study matrix failure at the microscale. The material parameters for the classical CDM model are directly obtained from physics-based atomistic simulations, thus improving the accuracy of the multiscale approach.

Introduction

Composite materials containing nanoparticles dispersed in the matrix medium exhibit improved performance and are emerging as one of the most promising areas in materials research associated with numerous aerospace applications. The mechanical behavior of nanocomposites and their individual constituents have been modeled and studied at various length and time scales. In recent years, molecular

Address correspondence to E-mail: nsubram7@asu.edu

DOI 10.1007/s10853-017-1733-y

simulations have gained traction in understanding the physical and chemical interactions between the various constituent phases of nanocomposites, resulting in an enhanced understanding of their structure–property relationships [1, 2]. Using molecular dynamic (MD) simulations, Koo et al. recently simulated the chemical curing of epoxy polymer by setting a cutoff distance between the active sites of the resin and the crosslinker molecules. When the active sites approach closer than the predefined cutoff distance during equilibration, appropriate bond information was assigned to the sites. [3]. Subramanian and co-workers investigated an epoxy system with dispersed CNTs and quantified the effects of the polymer cross-linking density and CNT weight fraction on linear elastic mechanical properties [4]. An exhaustive review of nanoscale modeling approaches shows that MD and Monte Carlo (MC) methods have been successful in determining the elastic mechanical properties of polymeric nanocomposites [5].

Although the elastic behavior of CNT nanocomposites has been investigated through experiments and computational efforts [4–7], fundamental mechanochemical interactions at the nanoscale that manifest as inelastic response at the continuum level are not yet well understood. Amorphous polymers at temperatures well below their glass transition temperature ($T \ll T_g$) exhibit brittle behavior whereas semicrystalline polymers tend to exhibit ductile behavior prior to failure at temperatures that fall between melting and glass transition ($T_m < T < T_g$), thus, clearly highlighting the difference in damage initiation mechanisms in crystalline and amorphous materials. Fundamental research on the origin of polymer failure was conducted by Mott et al. who investigated the molecular mechanisms that cause plastic behavior in glassy polymers through atomistic models [6]. Extensive studies by Rottler and Robbins shed light into damage nucleation mechanisms such as the segmental motions in the polymer chain that causes plastic flow followed by fully developed plastic events in the molecular system and bond dissociation leading to craze formations [7, 8]. A study performed by Lyulin and co-workers employed atomistic simulations to capture and compare the strain hardening and softening moduli among ductile polycarbonate and brittle polystyrene [9]. The authors studied segmental mobility and local dynamics to correlate the role of the polymer structure and intra/intermolecular interactions on the mechanical behavior of the material. Yashiro and co-workers used MD to study the nucleation of chain entanglements in long-chain polymers under uniaxial tension by employing a united model [10]. The results attributed the strain hardening phenomenon to the extension and entanglement of molecular chains of different orientations. However, bond dissociation occurring past the yield stress was not considered in both these studies, and the effects of bond rotation and van der Waals interactions alone were addressed. Roy and co-workers investigated the nonlinear behavior of polymers through molecular simulations using the atomistic J-integral based on Hardy estimates of continuum stresses [11]. While a few approaches involving the use of the finitely extensible nonlinear elastic (FENE) force field [12] have captured fracture successfully, the strains at which failure is observed do not correlate with experimental results.

To model strain softening and subsequent material degradation leading to damage at the microscale, several approaches have been explored to date. De Borst and Sluys computed the width of a finite plastic localization zone and the corresponding dissipation energy for an elasto-plastic, strain-softening Cosserat continuum [13]. The study incorporated a von Mises plasticity model formulated within the framework of a Cosserat continuum. Sayers and Kachanov developed an approach to estimate the elastic stiffness tensor for an arbitrary orientation distribution of cracks at finite crack densities [14]. Their approach relied on a tensorial transformation of the effective elastic constants for isotropic orientation statistics through the use of a second-order crack density tensor. Recent studies have shown the successful implementation of a continuum damage mechanics (CDM) model within a simple multiscale framework for composite materials, especially to examine matrix failure [15, 16]. However, most of the studies detailed here use homogenization approximations, such as the Mori–Tanaka method, to estimate the effective degraded material properties at damage sites.

A recent study by the authors on the simulation of molecular chain sliding and bond breakage in neat epoxy polymer demonstrated the use of a novel, computationally feasible MD approach as an alternative to expensive zero-temperature simulations [17]. In this paper, we extend the use of this atomistic simulation approach to investigate CNT-enhanced epoxy systems and further integrate the nanoscale

results to a comprehensive micromechanics-based matrix failure model. A hybrid force field MD simulation methodology is adopted to form cross-link bonds between the resin and the crosslinker molecules in the presence of CNTs, and to simulate damage initiation. The effect of thermal vibration of bonds on the strain applied at the nanoscale is investigated, following which the bond vibration frequency of a few individual bonds is calculated from the simulations. The correlation between temperature and strain rate of the simulation, and the corresponding variations in potential energy observed in the epoxy polymer system during post-yield deformation are also addressed. Zero-temperature simulations based on the quasi-continuum approach are used to estimate the long-term spatial and temporal average of the atomic virial stresses, which eventually converges to the value of the continuum Cauchy stress [18]. However, zero-temperature simulations are computationally intensive and time consuming. An approach whereby a combination of high strain rate and low-temperature MD simulations is performed to extract bond dissociation energy is adopted in order to better understand damage initiation [17]. The dissipated energy due to bond breakage calculated at the atomistic level is used to develop a material parameter that defines damage at the continuum level. This material parameter describes the degree of damage in various sections of the epoxy polymer in the form of a new constituent with degraded material properties; hence, this continuum approach simulates damage in an explicit manner at the microscale. This multiscale framework integrating a computationally efficient numerical approximation to a physics-based damage initiation phenomenon, and a continuum damage mechanics model provides valuable insights into damage precursor and performance of nanopolymers.

Molecular model

The epoxy polymer—EPON 862, used in this study, contains Di-Glycidyl Ether of Bisphenol F (DGEBF) as the resin constituent and Di- Ethylene Tri-Amine (DETA) as the crosslinker constituent. The ratio of constituents by weight in the simulation is consistent with the mixing ratio of the resin and the crosslinker used in the laboratory. The simulation volume consists of randomly dispersed CNTs among the resin and crosslinker molecules (230 molecular chains of DGEBF and 192 chains of DETA—determined based on the mixing ratio), and subsequently, the epoxy is cured in the presence of the CNTs. Figure 1 shows a cured epoxy system containing randomly dispersed CNTs (3 wt% CNT). All simulations are performed on the open-source molecular simulation platform, LAMMPS [19]. Multiple all-atom force fields, OPLS (Optimized Potentials for Liquid Simulations) and CVFF (Consistent Valence Force Field) for CNTs [20] and MMFF (Merck Molecular Force Field) for the epoxy polymer [21], are used to capture near-equilibrium interactions of the molecules in the elastic regime. The epoxy curing simulation employs a stochastic cutoff distance approach as described in the previous section of this paper [3]. The probability distribution of cross-linking degree for the polymer system and the variation of mechanical properties with cross-linking degree has been characterized in a previous work by the author [4]. Although the CNTs in the molecular simulation are not functionalized and chemically bonded to the surrounding polymer, the van der Waals forces between the CNTs and the epoxy are fully considered. The effects of the addition of CNTs in the epoxy matrix on the overall elastic properties such as Young's modulus, bulk, and shear moduli of the nanocomposite are discussed in Subramanian et al. 2015.

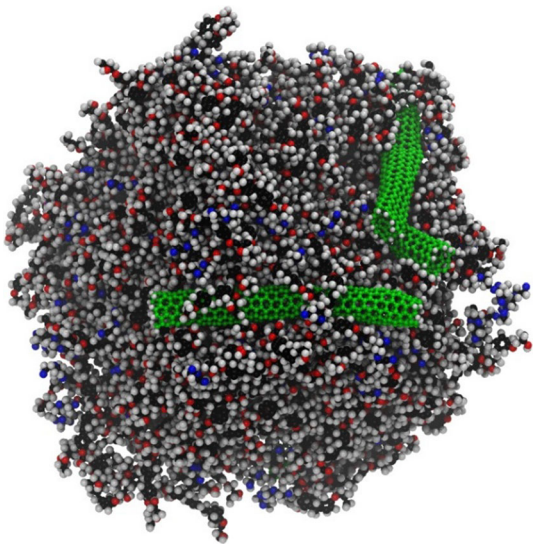

Figure 1 CPK representation of a simulation cell with cured epoxy polymer with randomly dispersed CNTs.

Classical force fields are not capable of capturing behavior occurring farther from equilibrium bond length leading to plasticity. Classical force fields assume a quadratic form that leads to an increase in bond energy with elongation of bonds. Bond order-based force fields, on the other hand, assume a critical bond length beyond which the energy curve flattens out, indicating the dissociation of the bond. The covalent bonds elongate during deformation and transfer the external forces from one molecule to another in the CNT and the matrix. Therefore, quantifying the effective local force in the deformed thermoset matrix helps in identifying covalent bond breakage, which manifests as brittle behavior of the material system at continuum scales. Classical force fields are employed in this study to simulate epoxy curing whereas a bond order-based potential is introduced to capture bond elongation and subsequent dissociation of covalent bonds. Bond order-based potentials use an enormous amount of time to perform curing/bond formation and bond order update on a bulk polymer system. The cured and equilibrated thermoset bulk polymer system obtained with classical MMFF and OPLS has accurate configuration; this has been validated by comparing the glass transition temperature (T_g) estimated by classical MD for the thermoset with experiments [3]. The authors are aware of the issues that arise from integrating and switching between potentials. Therefore, after the final cured configuration is obtained from the classical MD simulations, the unit cell is thoroughly equilibrated for 10 ns with the bond order-based potential to ensure a consistent molecular configuration and avoid unstable dynamics. The potential energy contributions from pair interactions do not vary between classical and reactive potentials because they both use similar formulations to calculate the energy from van der Waals interactions. Therefore, the pair energy difference of the same system at the beginning and at the end of equilibration was calculated using classical and reactive force fields, and was matched to a tolerance of 1E − 2 kcal/mol.

There are several bond order potentials such as Tersoff potential, Brenner potential, REBO/AIREBO potential, and ReaxFF. These potentials have been employed in studies depending on the materials of interest. For this study, ReaxFF is chosen because it is developed/optimized to simulate hydrocarbon compounds (such as CNT/epoxy nanopolymers). Since ReaxFF has many different parameter sets depending on types of hydrocarbon compounds, suitable parameters set should be carefully determined to obtain reliable simulation results. [22–26]. It is true that the most optimized set of potentials (as found in literature) for a specific material system can be obtained only through DFT-based studies. However, the aim of our study is not to determine the most optimized set of parameters for our nanopolymer system, but rather to use the most suitable bond order-based potential from existing parameter sets, since our length scales of interest do not extend to subatomic quantum calculations. A specific C-H bond in a CNT with end-Hydrogen atoms is stretched using the 'fix move' command while the rest of the system is equilibrated. As the bond breaks, the corresponding bond dissociation energy (BDE) is estimated from the simulation.

The BDE calculated from MD simulations using different ReaxFF potentials is compared to the C–H bond strength in CNTs as reported in the literature. The bond strength of the C–H bond in CNTs was calculated using DFT to be − 2.39 eV (equivalent to − 55.11 kcal/mol) as reported in the literature [27]. The bond dissociation energy calculated through MD simulations employing different bond order-based potential parameter sets is tabulated in Table 1. Based on the values in Table 1, the force field parameter set reported by Singh and co-workers matches best with DFT results. Since the error for the chosen parameter set is under 3.5%, this choice is sufficiently accurate for our study and will be employed in all the deformation simulations in this paper.

Thermal vibration of bonds

The application of temperature to a molecular system excites the system and causes the atoms to vibrate about their mean positions. The increase in temperature leads to an increase in the amplitude of

Table 1 BDE from various ReaxFF potential sets

Bond order-based potential	BDE (kcal/mol)
Chenoweth et al.	− 86.45
Weismiller et al.	− 89.66
Singh et al.	− 57.04
Mattsson et al.	− 145.22

molecular vibrations. In polymers, thermal degradation occurs when the energy of vibration exceeds the primary bonding between atoms, while the transitional phenomena associated with glass transition are related to rotation and vibration of molecular chains [28]. The frequency of vibration of a bond is directly proportional to its strength. For example, a C–C bond has a lower bond vibration frequency than a C–H bond. The higher the bond vibration frequency, the higher the energy required for breaking the bond. When a simulation volume is deformed by an external force, the new position of the atoms and the extension/contraction of the bonds in the system are dictated by the local force experienced by the atoms; however, it has been demonstrated in our previous work that the bond length variation is re-equilibrated between timesteps due to thermal vibration [17]. This re-equilibration of bond lengths is attributed to the frequency of bond vibrations being much higher than the rate at which the strain is experienced by the simulation volume. Therefore, in order to efficiently simulate bond elongation and dissociation between atoms, the effect of thermal vibration needs to be decoupled from the mechanical strain imparted to the simulation volume. It is important to note that the strain in the simulation volume is not equal to the macroscopic strain observed during a deformation test.

The bond vibration frequencies of several bonds in the constituent material system are investigated first. In order to calculate the bond vibration frequency, the molecular system is equilibrated in an NPT ensemble for 100 ps at 300 K and 1 atm. Several bonds of interest are chosen, and their equilibrium bond lengths are identified. During equilibration, the rate of bond length fluctuation is inverted to obtain frequency using fast Fourier transform (FFT). In the frequency domain, the peak value corresponds to the primary vibrational frequency of the specific bond. Since this investigation involves only an equilibration process, classical MD simulations are capable of extracting the bond vibration frequency. The bond stretching vibration frequency calculated for a carbon–carbon double bond (C=C) using FFT is shown in Fig. 2.

The C=C bond vibration frequency in ethene calculated from the aforementioned technique is 51.56 THz. This technique to calculate the bond stretching vibration frequency from bond length variation during equilibration is validated by

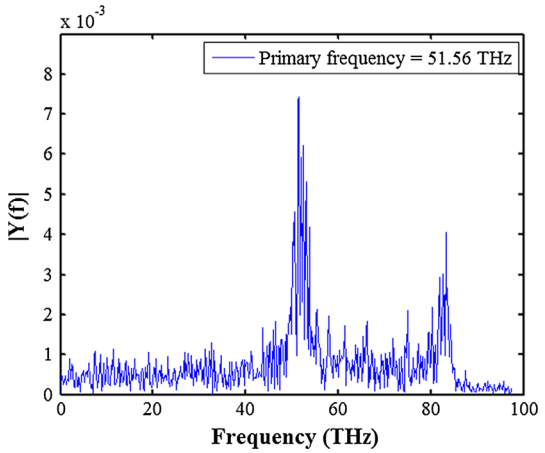

Figure 2 Bond stretching vibration frequency at 300 K for C=C bond in ethane.

comparing the frequency value to spectroscopy data published in the literature. Based on the results from spectroscopy, the C=C bond frequency in ethane was found to be about 49.2–51 THz [29]. The bond stretching vibration frequency analysis is further extended to specific bonds in the CNT-epoxy system, and the results are summarized in Table 2. The calculation of bond stretching vibration frequency provides better insight into thermally induced vibration in the system. In the following sections, the values of bond vibration frequency will be used as a guideline to develop a computationally efficient numerical framework to simulate bond breakage in the CNT-polymer system.

Fracture at the atomic scale

The importance of atomic-scale effects on microscopic fracture has been well recognized over the past few decades, yet the focus of even recent research has been limited to the understanding of atomic scale fracture in crystalline lattice-based material systems such as metals [30] and graphene [31]. Karger-Kocsis provided an analytical formulation to study the influence of fundamental molecular variables on the essential work to fracture in amorphous polymers; however, the essential work to fracture was not quantified using a discrete molecular model [32]. In order to relate discrete atomic level parameters to a continuum phenomenon called fracture, approaches that assume an embedded atomistic crack tip in a bulk continuum material have been widely adopted.

Table 2 Bond stretching vibrational frequency at 300 K for various bonds in the unit cell

Bond type	Bond vibrational frequency (THz)
C=C (sp2, CNT)	21.48
C–H (sp3, CNT)	63.48
C–C (benzene ring, resin); data from [17]	33.45
C–O (resin); data from [17]	38

The deformation of crystalline materials is founded on the Cauchy–Born approximation, a hypothesis that relates the movement of atoms in the crystal lattice to the overall deformation in a bulk solid. The atomistic deformation of the lattice follows the same trend as continuum deformation due to fixed equilibrium distances between atoms. This method serves as a mapping technique for strain from the continuum mechanics framework to the discrete atomic framework. This assumption, however, is not appropriate for amorphous material systems, and the displacement of atoms does not follow the overall deformation in the bulk solid. The molecular chains in amorphous materials are not arranged in an ordered fashion, and the deformation of the unit cell does not cause a proportional stretching of the chains. Instead, the local force experienced by atom clusters dictates the motion and displacement of individual atoms and molecules in amorphous solids.

Zero-temperature MD simulations

In the LAMMPS framework, the zero-temperature simulation algorithm based on the quasi-continuum concepts presented by Tadmor et al. simulates quasi-static loading discarding temperature effects and uses energy minimization to find ground-state configurations at each strain step [33]. The simulation volume is deformed using the 'change_box' command; the coordinates of atoms in the volume are remapped from a previously unit cell volume shape/size to a new one using an affine transformation [34, 35]. The method is also able to simulate an absolute zero-temperature condition in the atomic system thereby discarding all the effects of thermal vibration of bonds. Thus, the zero-temperature simulation approach is appropriate for investigating bond elongation and bond breakage due to pure mechanical loading. However, the energy minimization associated with each strain step makes the method computationally intensive and time consuming. A CNT-epoxy unit cell with 25,700 atoms is constructed, and the zero-temperature method is applied to the unit cell for 10000 tensile strain steps. A computing node on the high-performance computing cluster using eight CPU cores was used to perform this simulation, which lasted a total wall clock time of over 100 h. The prohibitively large computational time associated with zero-temperature MD simulations warrants the use of a numerical framework that can simulate fracture in amorphous solids in a reliable and computationally efficient manner.

Ultra-high strain rate approach to capture bond dissociation

The addition of heat increases the amplitude of vibration of atoms, and the kinetic energy also causes the atomic bonds to stretch and relax about their equilibrium lengths. In order to mitigate the influence of bond vibration on bond elongation in amorphous materials, and to provide an alternative to the computationally intensive zero-temperature simulation method, two approaches are explored in this paper. The first approach implements MD simulation with hybrid force fields (empirical force field for equilibration and curing, and bond order-based force field for deformation and bond breakage) at near-zero temperatures. The second approach uses MD simulation to perform deformation tests at extremely high strain rates. These strain rates are higher than the average bond vibration frequency; hence, the application of successive strain steps occurs faster than bond vibrations, and thus, thermal effects cannot re-equilibrate the lengths of bonds in the system.

A tensile deformation simulation is performed on a unit cell with 3% CNT by weight imposed with periodic boundary conditions. The CNTs are randomly dispersed among the resin and crosslinker molecules with no covalent bonding. The CNTs are short ($\sim$ 100 nm in length) and have a diameter of $\sim$ 10 nm; they are open-ended, and the end carbon atoms are hydrogenated to ensure thermal stability. An absolute zero-temperature condition leads to zero kinetic energy, and the atoms in the system cannot move; therefore, MD simulations are not possible at zero temperature. Here, subsequent to the

equilibration of the system for 100 ps, with a timestep of 1 fs, in an NPT ensemble at 1 atm pressure and near-zero temperature ($\sim$ 1 K, controlled by a Nose–Hoover thermostat), a tensile deformation is performed until 100% strain, and the corresponding temperature value and variation in potential energy resulting from elongation, distortion, and dissociation of bonds are calculated at each strain step. Figure 3 illustrates the variation in potential energy during the tensile deformation simulation performed at different strain rates ranging from 1×10^{9} s^{-1} to 1×10^{12} s^{-1}.

The temperature at the end of the equilibration stage is calculated to be 1.86 K, following which the tensile deformation is applied on the simulation volume at different strain rates. For higher strain rate cases, the fluctuation of temperature during the application of strain is higher. This high fluctuation is because the magnitude of applied perturbation (strain, in this case) from the equilibrium state is larger for high-strain rate simulations. Thus, low strain rate simulations with a lower magnitude of perturbation, and a longer run-time maintain a value of temperature close to the target temperature, whereas high strain rate cases are only able to achieve a stable temperature of 5.89 K. Typically, an increase in temperature is expected to raise the kinetic energy of the system; however, the kinetic energy induced in the system could lead to multiple modes of vibration such as bond stretching, bond angle bending, and bond dihedral and bond improper torsion. These geometric changes could increase the potential energy of the system, although this change may not be as significant as the change in kinetic energy.

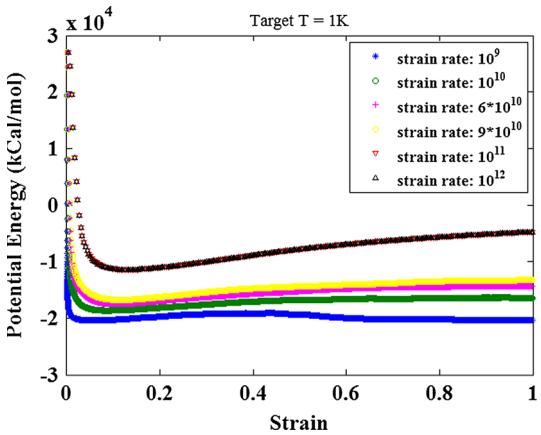

Figure 3 Potential energy variation during tensile deformation at different strain rates.

In order to quantify the effect of temperature on potential energy variations caused by geometric distortions, MD simulations were performed with equilibration at two different temperatures—1 K and 300 K. The tensile deformations were applied at multiple strain rates at these two temperatures. Figure 4a–d shows the variation of potential energy with strain at different strain rates ranging from 1×10^{11} s^{-1} to 1×10^{14} s^{-1}.

The plots illustrate that the systems that were equilibrated at a higher temperature possess higher potential energy during the initial steps of the tensile test although the simulation volume was constructed with the same initial configuration of molecules. This phenomenon is seen to be true at all strain rates that were applied. The variation in potential energy due to increase in the average temperature of the molecular system confirms the hypothesis that temperature indirectly contributes to an increase in potential energy by causing geometric bond distortions as a result of atomic vibrations. The trends observed from Fig. 4a–d are the result of two distinct mechanisms contributing to the variation in potential energy: (1) the increase in temperature (by adding kinetic energy) causes geometric distortions in the molecular system due to more vibration and indirectly leads to an increase in potential energy, and (2) the addition of strain to the simulation volume leads to bond length variations and a corresponding change in potential energy.

In Fig. 4a and b, the applied strain rate is lower than the vibrational frequency of bonds at $\sim$ 1 K and 300 K; therefore, the applied strain does not result in potential energy changes because the bonds get re-equilibrated, i.e., the effect of (1) is more significant than that of (2). At higher strain rates ($\sim$ 10^{13} s^{-1}), as shown in Fig. 4c and d, the applied strain rate exceeds the bond vibration frequencies in the $\sim$ 1 K and the 300 K simulations, thus, weakening the influence of averaged temperature measured by the thermostat of the molecular system. The applied strain on the unit cell translates to the elongation of the atomic bonds when the strain rate of deformation is higher than bond frequency and the effects of (2) are more dominant than that of (1). Figure 4d illustrates the convergence of the potential energy values of the two CNT-epoxy systems despite their average temperature being different, indicating that the increase in potential energy with strain is invariant to temperature. The thermostat becomes ineffective

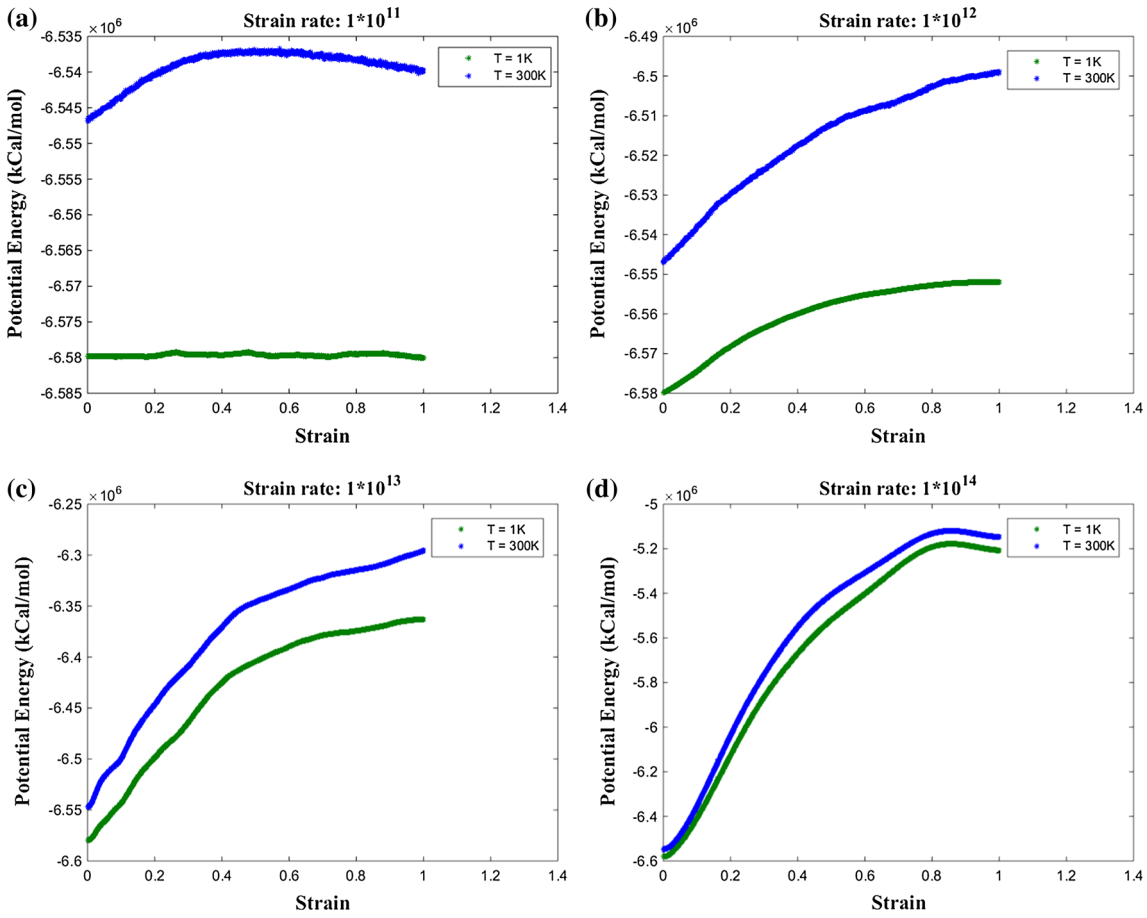

Figure 4 Thermal effects on potential energy at strain rate: **a** 1×10^{11}/s, **b** 1×10^{12}/s, **c** 1×10^{13}/s, **d** 1×10^{14}/s.

because the thermal vibrations are decoupled from the mechanical deformation. For example, the raw stress–strain data from simulations at ~ 1 K at two different strain rates—10^{11} s^{-1} and 10^{14} s^{-1} of a system with 3% CNT wt are presented in Fig. 5. The noise in the 10^{11} s^{-1} simulation arises from thermal vibrations. Also, note that the stress–strain curve does not drop with increase in strain; this forms the basis of our initial claim that bond breakage does not occur at this strain rate. Although the chosen ReaxFF potential is appropriate, bond breakage is not observed because thermal fluctuations tend to re-equilibrate the bond lengths; thus, the strain imposed on the simulation volume is not imparted to the bonds at strain rate of 10^{11} s^{-1}. However, the raw data from the 10^{14} s^{-1} simulations is smooth indicating that the thermal effects have been decoupled, and what is observed is a quasi-continuum-equivalent deformation of the molecular system. This ultra-high strain rate required to decouple thermal effects varies from one material system to another and needs

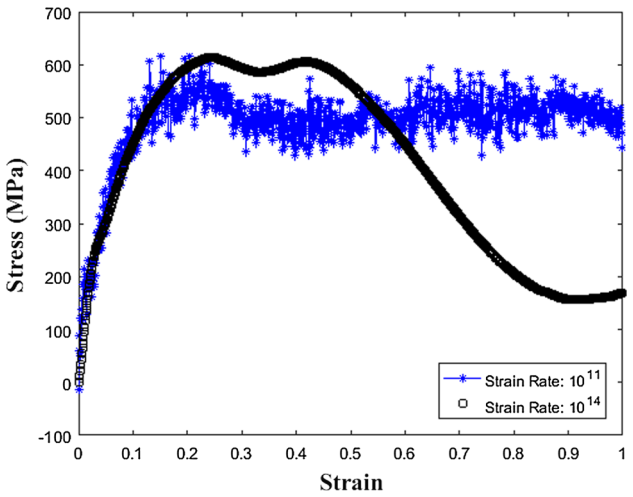

Figure 5 Raw stress–strain data from MD simulations at 10^{11} s^{-1} and 10^{14} s^{-1} of the same molecular system.

to be independently found for each material system. Simulations to model bond dissociation in amorphous polymers with dispersed CNTs can now be

performed even at finite temperatures without a computationally intensive zero-temperature simulation method.

The stresses in the MD simulations are obtained from the spatial and temporal averaging of virial stresses, and the deformation is imposed with a boundary strain method. The stress–strain response of the CNT-epoxy system from the virtual deformation test at 10^{14} s^{-1} strain rate is plotted in Fig. 6. During deformation, the covalent bonds elongate from their equilibrium lengths—this corresponds to the linear elastic portion of the stress–strain curve. A softening phenomenon subsequent to the yield point is due to stretching of molecular clusters and dissociation of the weaker covalent bonds. The first dip in the stress–strain curve corresponds to bond breakages initiating in clusters of low polymer cross-linking. Subsequently, the polymer chains become fully stretched and long chains slide relative to each other, resulting in the strain hardening phase. This is also the phase when the polymer chains transfer load to the CNTs and the elongation of CNTs are observed. Finally, when the polymer chains break due to quick, successive bond dissociation, there is not enough percolation for the CNTs to bear the load completely. This results in complete material failure.

Since chain sliding and bond dissociation are the fundamental origins of material fracture, it is possible to relate the variation of bond energy in molecular systems under deformation to damage precursors at the higher length scales. Bond energy increases due to bond elongation and decreases suddenly due to dissociation of the covalent bond. The variation of bond energy between the undeformed, unbound state of the molecular system and at each timestep of the deformation test is used to quantify the bond dissociation energy (BDE). The value of bond energy is recorded before the deformation simulation initiates; furthermore, as deformation occurs the bond energy lost (converted to pair energy) due to bond scission events is calculated and defined as BDE. Since the bond strength of each bond is known a priori, the number of bond scission events and their individual contribution to BDE per volume is defined as the bond dissociation energy density. Figure 7 illustrates the variation of BDE density with CNT weight fraction in the polymer matrix, for different strains, during the deformation test. The BDE density is used as a critical parameter in the microscale CDM model to define damage as described in the following section.

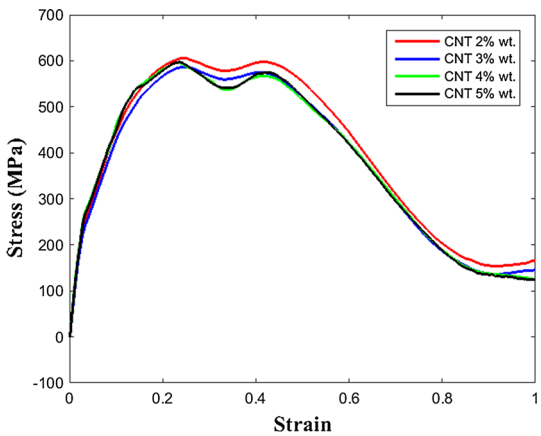

Figure 6 Stress–strain response from tensile test at 10^{14} s^{-1} strain rate.

CDM-integrated stochastic microscale model

The bond breakage information from the atomistic scale is transferred to the continuum scale to investigate matrix damage and failure. A simple CDM formulation is used to demonstrate the bridging mechanism. The BDE density due to bond breakage in the simulation volume calculated at the nanoscale is used to define a material parameter for damage at the continuum level. This material parameter transforms the damaged material in the continuum simulation to a new constituent with altered material properties. The multiscale CDM approach also makes computation in an FEA framework convenient as the need to develop exclusive damage elements, such as in extended FEM (XFEM), is averted.

From the BDE density quantified at the molecular level, a nonlinear curve fitting method is adopted to obtain a mathematical relationship between BDE density, CNT weight fraction in the epoxy matrix, and applied strain as described in Eq. (1), where B is the BDE density calculated from MD simulations, ρ is the weight fraction of CNT, and ϵ is the strain.

$$\begin{aligned} B(\epsilon,\rho) = {} & (p\rho^3 + q\rho^2 + r\rho + s)\epsilon^3 \\ & + (e\rho^3 + f\rho^2 + g\rho + h)\epsilon^2 \\ & + (i\rho^3 + j\rho^2 + k\rho + l)\epsilon \end{aligned} \tag{1}$$

A damage parameter d is formulated to define and quantify material degradation as follows.

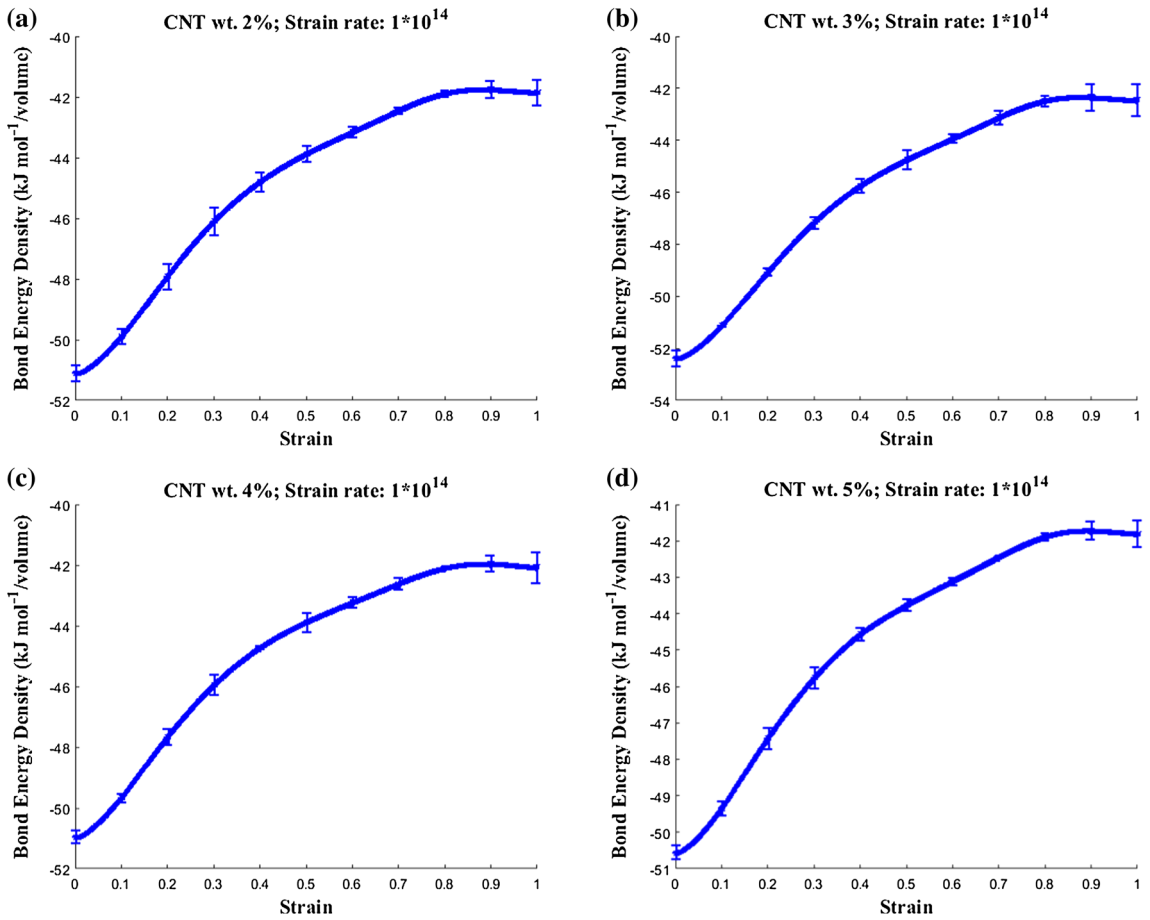

Figure 7 Variation of BDE density with CNT weight fraction and strain. **a** 2% CNT wt, **b** 3% CNT wt, **c** 4% CNT wt, **d** 5% CNT wt.

$$d = \frac{B(\epsilon, \rho) - B_{ip}}{B_c - B_{ip}} \tag{2}$$

B_c, in Eq. (2), represents the critical value of BDE density at which the material loses load carrying capacity; in this work, B_c is the point where the tangent to the curve made by B with respect to the variation of strain $(\partial B(\rho, \epsilon)/\partial \epsilon)$ is zero. B_{ip} denotes the BDE density corresponding to the onset of damage in the material. It is estimated as the BDE density at the elastic limit of the material from the MD simulation stress–strain curves.

$$B_{ip} = B\left(\epsilon^i_{\left|\frac{\partial^2 \sigma}{\partial \epsilon^2}\right| > 0}, \rho\right) \tag{3}$$

The BDE density required to initiate brittle response is the critical value at which the second differential of the stress–strain curve exceeds zero $(\partial^2\sigma/\partial\epsilon^2 > 0)$. At the continuum level, a damage tensor is introduced, which can be simplistically defined along the principal directions for the special case where the loading direction is consistently parallel along the principal directions; the damage parameter defined along each principal direction is calculated as a function of the weight fraction of CNT and the principal strain along the direction at the current timestep. Although each damage parameter is a function of the strain in that direction, the damage function that each damage parameter follows is the same. It should also be noted that the pristine polymer and nanopolymer systems are isotropic at the continuum level. Hence, the material constitutive matrix can be easily calculated using two material constants calculated from MD simulations; however, directional damage in the nanopolymer may lead to a non-isotropic system. For example, a uniaxial load produces a three-dimensional strain state due to Poisson's effect, three damage parameters evolve, one for each principal direction as a function of the strain along that direction. A biaxial load will act as a superposition of uniaxial loading states, and the damage evolution will also be a superposition of uniaxial cases with corresponding Poisson's coupling effects.

The principle of strain equivalence, as shown in [15] and [16], is used to formulate the degraded elastic material properties as a function of the damage parameters. $\bar{E}_i$ and $\bar{v}_i$ are the degraded material properties whereas E_p and v_p represent the pristine material properties of the CNT-enhanced epoxy system. The softened material properties are further employed to formulate the kinematics and update the material constitutive equations.

$$\bar{E}_i = E_p(1 - d_i) \tag{4}$$

$$\overline{v_i} = v_p\left(1 + d_i\left(\frac{0.5}{v_p} - 1\right)\right) \tag{5}$$

The fundamental piece of the stochastic microscale continuum model is a cubic unit cell corresponding to an epoxy matrix element. Each epoxy cubic element of the RVE is characterized by unique material properties to incorporate stochasticity in CNT weight fraction and polymer cross-linking density. The stochastic microscale model and the corresponding sampling methods employed to characterize the stochasticity are explained in detail in [4]. A 3D array of unit cells with periodic boundary conditions constitutes a representative volume element (RVE) for the model. Figure 8 illustrates a 3D RVE containing 1000 epoxy matrix cells ($10 \times 10 \times 10$ unit cells) accounting for the uncertainty in CNT weight fraction in the epoxy matrix. It is important to note that the color scheme in Fig. 8 is merely a representation of stochasticity. Due to the random sampling process, no two unit cells will likely have the same CNT weight fraction and polymer cross-linking degree (although some colors are repeating in the figure).

The CDM equations are integrated into the stochastic microscale model to evaluate the damage and subsequent failure of the microscale RVE under uniaxial tensile loading. The normalized damage parameter for each epoxy section varies between 0 (pristine) to 1 (fully damaged). Figure 9a, b shows the damage parameters and the stress–strain curve calculated for an RVE when the stochastic microscale model with the CDM formulation is implemented with a mean CNT weight fraction of 2, 3, and 4%. It is evident that the RVE exhibits nonlinear behavior at low strains, indicating the presence of inelasticity. The damage parameter increases steeply until a critical strain of 10–15% is reached, followed by a flattening trend. It is important to note that in general epoxy polymers fail at much lower strains during experiments. The authors hypothesize that this discrepancy could be due to the presence of voids and other local variations which are not included in this analysis. However, the integration of this model into a high-fidelity multiscale damage framework shows good correlation with experiments and several other numerical damage models such as the Lemaitre CDM model and the Gurson–Tvergaard–Needleman (GTN) damage model [36]. The comparison of the MD-integrated CDM model correlated accurately with physical evidence that damage evolution initiates at a slow rate, but gets accelerated as cracks coalesce and slows down subsequently as the damaged state saturate. The results from this study indicate that an increase in CNT weight fraction improves the elastic and inelastic properties of the nanopolymer, as seen from the stress–strain curves; however, the critical strain for damage rate increase

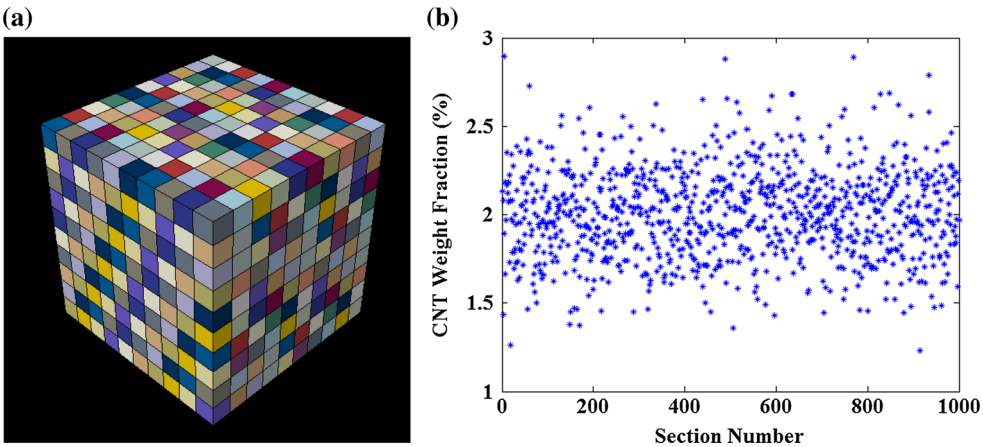

Figure 8 **a** RVE in the stochastic microscale continuum model, **b** sampled CNT weight fraction values for each section.

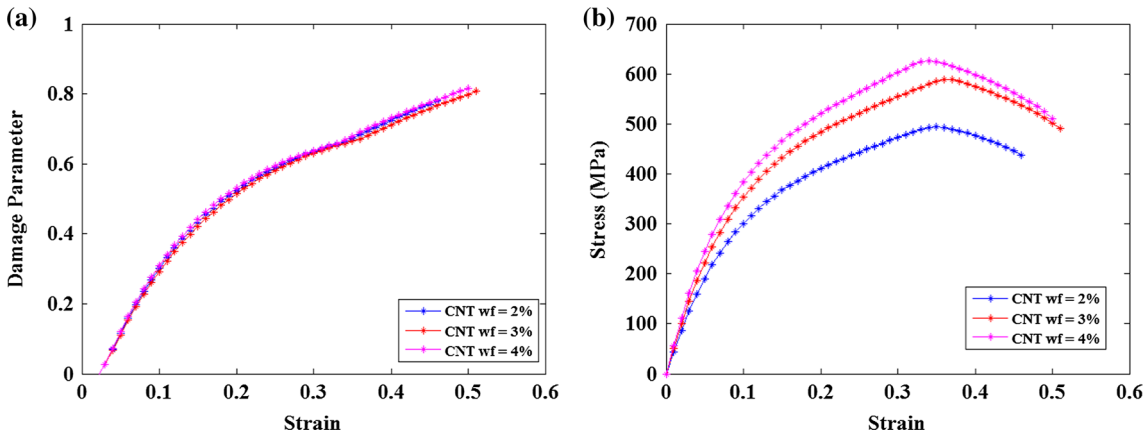

Figure 9 **a** damage parameter values, **b** stress–strain curves for microscale RVE.

remains unchanged. Thus, it is reasonable to conclude that the initiation of damage is more closely attributed to the matrix properties than the inclusion of CNTs.

Conclusion

A numerical methodology was developed to simulate bond breakage and damage initiation in amorphous polymeric systems with dispersed CNTs. The study primarily addressed the effects of temperature-induced bond vibrations on the molecular system during deformation simulations. It was evident that bond vibrations led to relaxation of bonds and reduced the probability of bond dissociation during tensile simulations. An alternative technique to the zero-temperature simulation method, previously developed by the authors, that enables the study of bond dissociation by decoupling the effects of temperature and strain was extended to characterize damage in CNT-epoxy systems. We reiterate that this method is not focused on capturing the high strain-rate response of the CNT-dispersed polymer; the paper only uses the ultra-high strain-rate method as a computational alternative to simulate quasi-continuum response. This idea is similar to employing the quasi-continuum method as an alternative to unphysical zero-temperature simulations for studying materials free from any thermal effects. The MD simulations at near-zero temperatures revealed that temperature also causes an indirect increase in potential energy by inducing geometric distortions to molecular structure. Additionally, the effects of temperature and strain on the variation in potential energy were quantified and decoupled by exploring high strain rate ranges for MD simulations. The tensile deformation simulations performed using a combination of low temperature ($\sim$ 1 K) and high strain rate ($\sim 10^{13}\ s^{-1}$) not only allow to observe bond breakage but also offer significant computational advantages. This alternative methodology also provides a platform to quantify the BDE in the molecular system and capture the brittle fracture regime of the CNT-dispersed polymer.

The CDM method was modified to account for atomistically obtained BDE data. A stochastic microscale continuum model was implemented based on CDM using the BDE density obtained at the nanoscale. The damage parameter in the continuum model was defined based on the energy dissipated in the amorphous molecular system from the elongation and subsequent dissociation of bonds. The stochastic microscale model captured the effects of local variations on the overall inelastic response and damage initiation in the nanopolymer. Results indicate that the inclusion of CNTs improves the overall mechanical response of the nanopolymer; however, the damage initiation phenomenon in CNT-enhanced epoxy polymers is primarily driven by the physics and chemistry of the polymer arising from a fundamental level due to the elongation and dissociation of covalent bonds.

Acknowledgements

This research was funded by the Office of Naval Research (ONR), Grant Number: N00014-14-1-0068. The program manager is Mr. William Nickerson.

Compliance with ethical standards

Conflict of interest The authors declare that they have no conflict of interest.

References

[1] Zeng Q, Yu A, Lu G (2003) Molecular dynamics simulation of organic–inorganic nanocomposites: layering behavior and interlayer structure of organoclays. Chem Mater 15(25):4732–4738

[2] Jancar J, Douglas J, Starr FW (2010) Current issues in research on structure–property relationships in polymer nanocomposites. Polymer 51(15):3321–3343

[3] Koo B, Liu Y, Zou J (2014) Study of glass transition temperature (T_g) of novel stress-sensitive composites using molecular dynamic simulation. Modell Simul Mater Sci Eng 22(6):065018

[4] Subramanian N, Rai A, Chattopadhyay A (2015) Atomistically informed stochastic multiscale model to predict the behavior of carbon nanotube-enhanced nanocomposites. Carbon 94:661–672

[5] Valavala P, Odegard G (2005) Modeling techniques for determination of mechanical properties of polymer nanocomposites. Rev Adv Mater Sci 9:34–44

[6] Mott P, Argon A, Suter U (1993) Atomistic modelling of plastic deformation of glassy polymers. Philos Mag A 67(4):931–978

[7] Rottler J, Barsky S, Robbins MO (2002) Cracks and crazes: on calculating the macroscopic fracture energy of glassy polymers from molecular simulations. Phys Rev Lett 89(14):148304

[8] Rottler J, Robbins MO (2003) Molecular simulations of deformation and failure in bonds formed by glassy polymer adhesives. J Adhes Sci Technol 17(3):369–381

[9] Lyulin A, Vorselaars B, Mazo M (2005) Strain softening and hardening of amorphous polymers: atomistic simulation of bulk mechanics and local dynamics. EPL (Europhys Lett) 71(4):618–624

[10] Yashiro K, Ito T, Tomita Y (2003) Molecular dynamics simulation of deformation behavior in amorphous polymer: nucleation of chain entanglements and network structure under uniaxial tension. Int J Mech Sci 45(11):1863–1876

[11] Roy S, Akepati A, Hayes N (2012) Multi-scale modeling of nano-particle reinforced polymers in the nonlinear regime. In: Proceedings of the 53nd AIAA-SDM Conference, Honolulu, HI

[12] Panico M, Narayanan S, Brinson L (2010) Simulations of tensile failure in glassy polymers: effect of cross-link density. Modell Simul Mater Sci Eng 18(5):055005

[13] De Borst R, Sluys L (1991) Localisation in a Cosserat continuum under static and dynamic loading conditions. Comput Methods Appl Mech Eng 90(1):805–827

[14] Sayers C, Kachanov M (1991) A simple technique for finding effective elastic constants of cracked solids for arbitrary crack orientation statistics. Int J Solids Struct 27(6):671–680

[15] Voyiadjis GZ, Kattan PI (2006) Damage mechanics with fabric tensors. Mech Adv Mater Struct 13(4):285–301

[16] Shojaei A, Li G, Fish J (2014) Multi-scale constitutive modeling of ceramic matrix composites by continuum damage mechanics. Int J Solids Struct 51(23):4068–4081

[17] Koo B, Subramanian N, Chattopadhyay A (2016) Molecular dynamics study of brittle fracture in epoxy-based thermoset polymer. Compos Part B Eng 95:433–439

[18] Subramaniyan AK, Sun C (2008) Continuum interpretation of virial stress in molecular simulations. Int J Solids Struct 45(14):4340–4346

[19] Plimpton S (1995) Fast parallel algorithms for short-range molecular dynamics. J Comput Phys 117(1):1–19

[20] Jorgensen WL, Maxwell DS, Tirado-Rives J (1996) Development and testing of the OPLS all-atom force field on conformational energetics and properties of organic liquids. J Am Chem Soc 118(45):11225–11236

[21] Zoete V, Cuendet MA, Grosdidier A (2011) SwissParam: a fast force field generation tool for small organic molecules. J Comput Chem 32(11):2359–2368

[22] Van Duin AC, Dasgupta S, Lorant F (2001) ReaxFF: a reactive force field for hydrocarbons. J Phys Chem A 105(41):9396–9409

[23] Chenoweth K, van Duin AC, Goddard WA (2008) ReaxFF reactive force field for molecular dynamics simulations of hydrocarbon oxidation. J Phys Chem A 112(5):1040–1053

[24] Weismiller MR, Duin ACV, Lee J (2010) ReaxFF reactive force field development and applications for molecular dynamics simulations of ammonia borane dehydrogenation and combustion. J Phys Chem A 114(17):5485–5492

[25] Singh SK, Srinivasan SG, Neek-Amal M (2013) Thermal properties of fluorinated graphene. Phys Rev B 87(10):104114

[26] Mattsson TR, Lane JMD, Cochrane KR (2010) First-principles and classical molecular dynamics simulation of shocked polymers. Phys Rev B 81(5):054103

[27] Wei C, Cho K, Srivastava D (2001) Chemical bonding of polymer on carbon nanotube. In: MRS Proceedings, vol 675. Cambridge University Press, Cambridge, pp W4. 7.1

[28] Ebewele RO (2010) Polymer science and technology. CRC Press, Boca Raton

[29] Lin-Vien D, Colthup NB, Fateley WG (1991) The handbook of infrared and Raman characteristic frequencies of organic molecules. Academic Press, San Diego

[30] Miller R, Tadmor E, Phillips R (1998) Quasicontinuum simulation of fracture at the atomic scale. Modell Simul Mater Sci Eng 6(5):607–638

[31] Zhao H, Aluru N (2010) Temperature and strain-rate dependent fracture strength of graphene. J Appl Phys 108(6):064321

[32] Karger-Kocsis J (2000) Microstructural and molecular dependence of the work of fracture parameters in semicrystalline and amorphous polymer systems. Eur Struct Integr Soc 27:213–230

[33] Tadmor EB, Ortiz M, Phillips R (1996) Quasicontinuum analysis of defects in solids. Philos Mag A 73(6):1529–1563

[34] Basu A, Wen Q, Mao X (2011) Nonaffine displacements in flexible polymer networks. Macromolecules 44(6):1671–1679

[35] Sommer J, Lay S (2002) Topological structure and nonaffine swelling of bimodal polymer networks. Macromolecules 35(26):9832–9843

[36] Rai A, Subramanian N, Koo B (2016) Multiscale damage analysis of carbon nanotube nanocomposite using a continuum damage mechanics approach. J Compos Mater, 51(6):847–858